CIEPLNE MASZYNY PRZEPŁYWOWE
No. 122 TURBOMACHINERY 2002

Piotr LAMPART
Institute of Fluid Flow Machinery, Polish Academy of Sciences, Gdańsk, Poland,
e-mail: lampart@imp.gda.pl

Sergey YERSHOV, Andrey RUSANOV
Institute for Mechanical Engineering Problems,
Ukrainian National Academy of Sciences, Kharkov, Ukraine,
e-mail: yershov@ipmach.kharkov.ua;
FlowER ltd., Kharkov, Ukraine,
e-mail: flower@flower3d.org

VALIDATION OF TURBOMACHINERY FLOW SOLVER ON TURBOMACHINERY TEST CASES

A 3D RANS solver FlowER is supplemented with two turbulence models – algebraic model of Baldwin-Lomax and two-equation shear stress transport model of Menter - a relatively recently developed model that combines good features of the k-ω and k-ε turbulence models. The code is validated on a Durham low speed turbine cascade, transonic NASA compressor Rotor37, and NASA low speed centrifugal compressor - giving the comparison of computed and experimental flow patterns as well as efficiency and pressure ratio characteristics of these machines.

1. INTRODUCTION

Industrial CFD is under rapid development to become an industrial technology, for example in power or aerospace industry. However, the full potential of CFD in industrial design is still limited due to high required computational costs, possible numerical inaccuracy and uncertainty coming from modelling physical processes, for example turbulence. Direct Numerical Simulation or even Large Eddy Simulation in turbomachinery flows are still beyond the capability of the computing machines. Turbomachinery flow solvers draw on the RANS approach offering a variety of turbulence closures. Unfortunately none of them is perfect for a general case, however, some are capable to work well in certain geometries and flow regimes. This makes the task of validating computational results very important. The significance of validation of numerical results is expressed in the fact of holding annual or bi-annual ERCOFTAC Workshops on 3D Turbomachinery Flow Prediction where a number of turbomachinery test cases are considered. Well-documented experimental data from the test cases are used there to validate the computational results from different authors/flow solvers, see [1]. Turbomachinery CFD is also

part of the QNET-CFD Thematic Network where a number of application challenges, giving quality measurement results of turbomachinery geometries and underlying flow regimes, are put forward to provide a data base for validating computational results, see [2].

CFD codes continue to improve their properties and become equipped with better and better numerical schemes, grid capabilities and more advanced turbulent closures. With each new version of a code, well-documented flow geometries are recalculated anew to verify how the predictions improved, compared to the previous version. In this paper, a recent version of the turbomachinery flow solver FlowER is shortly described and newly validated on three popular turbomachinery test cases - Durham Low Speed Turbine Cascade, NASA Rotor37 and NASA Low Speed Centrifugal Compressor.

2. FLOW SOLVER

In the code FlowER developed by Yershov & Rusanov [3], 3D viscous compressible flow through a turbine/compressor stage is described by a set of unsteady Reynolds-averaged Navier-Stokes equations. The governing equations are supplemented either with a modified algebraic turbulence model of Baldwin-Lomax [4] or two-equation shear stress transport (SST) model of Menter [5]. In the latter, the standard k-ω model is activated in the near wall region, and then switched to the k-ε model near the edge of the boundary layer and in free shear layers. Also the eddy viscosity is redefined so as to guarantee the proportional relationship between the principal turbulent shear stress and the turbulent kinetic energy in the boundary layer. A number of test cases given by Menter [5] show that the model is able to predict well adverse pressure gradient flows.

The computations for this paper are carried out in one blade-to-blade passage of the stator and rotor, and converge to a steady state. The computational domain extends also on axial gaps and radial gaps above/below unshrouded blade tips. The governing equations are solved numerically based on cell-centred finite-volume discretisation, Godunov-type upwind differencing, high resolution ENO scheme, and δ implicit operator, see Yershov [6], also Yershov et al. [7]. The scheme is second-order accurate in space and time. An H-type grid refined near the endwalls, blade walls, trailing and leading edges is assumed.

3. DURHAM LOW SPEED TURBINE CASCADE (DLSTC)

This well-documented turbine cascade measured by Gregory-Smith [8] is a very popular turbomachinery test case, particularly suitable for tracing secondary flow vortices and loss mechanisms in turbine cascades. The exit Mach number for this cascade is equal to 0.1.

Fig. 1 shows the comparison of static pressure coefficient $((p_0-p)/0.5\rho v_0^2$, where p_0 is the inlet pressure, p - local pressure, $0.5\rho v_0^2$ - inlet dynamic head) at the pressure and suction surface of the blade at various distances from the endwall. The choice of computed sections follows from the assumed grid, and the computed sections are those near-

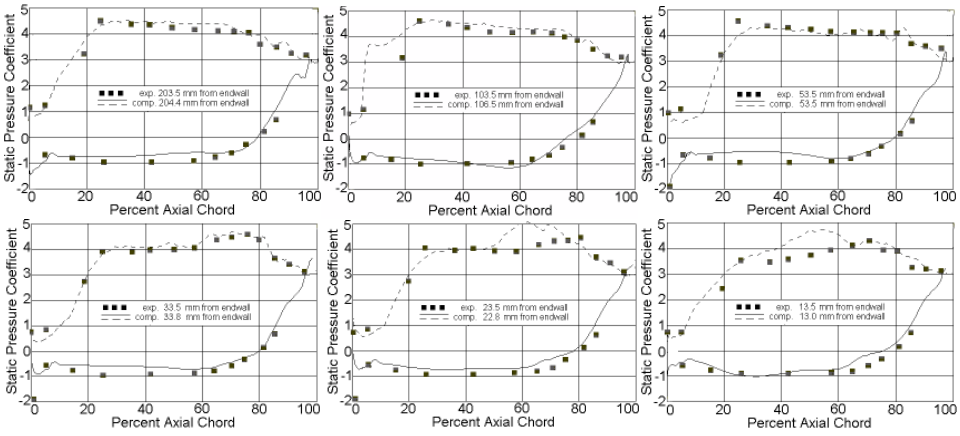

Fig. 1. DLSTC - static pressure coefficient at blade sections at various distances from endwall.

est to the measured sections. Anyway, the main tendencies in blade pressure profiles are reasonably well reproduced in the numerical results. The computed static pressure is slightly underestimated at the leading part of the suction surface at ¼ blade span (centre-top picture), and also slightly underestimated at the centre part of the suction surface near the endwalls (centre-bottom or right-bottom picture).

The comparison of experimental and computed secondary flow vectors (mid-span main-stream velocity subtracted) in an exit section located 28% downstream of the trailing edge, referred to as slot 10, is presented in Fig. 2. Please note that, unlike the experimental vectors, the computed velocity vector is not an arrow but consists of a dot and a stretch showing the direction of the velocity. Both pictures exhibit the presence of three vortices – a main big passage vortex, a counter-rotating suction surface shed vortex located top-left from the passage vortex, and a small corner vortex near the endwall. The main difference in the measured and computed field is here a smaller size (circumferential extension) of the passage vortex in the computational results. At the same exit section, Fig. 3 shows the comparison of experimental and computed total pressure coefficient ($(p_{0T}-p_{1T})/0.5\rho v_1^2$ – where p_{0T} is the inlet total pressure, p_{1T} – exit total pressure, $0.5\rho v_1^2$ - exit dynamic head). Besides the wake region, the three vortices described above are pronounced here as loss centres. The two discernible peaks due to the development and interaction of passage vortex and shed vortex seem to be underestimated in the numerical results. The computed passage vortex isolines occupy less space. However, the intensity of the third loss peak due to the corner vortex is computed correctly.

The presented computational results were obtained on a grid of 600 000 cells (showing no difference compared to those on 500 000 cells) using the algebraic closure of Baldwin-Lomax. Similar results for this cascade were obtained with the help of the more advanced two-equation SST model of Menter with the freestream turbulence intensity of 5% assumed as in the experiment. In the SST model the loss core due to secondary flows slightly moves towards the endwall, but still remains underestimated as in the case of the Baldwin-Lomax model. This can be seen from the comparison of span-

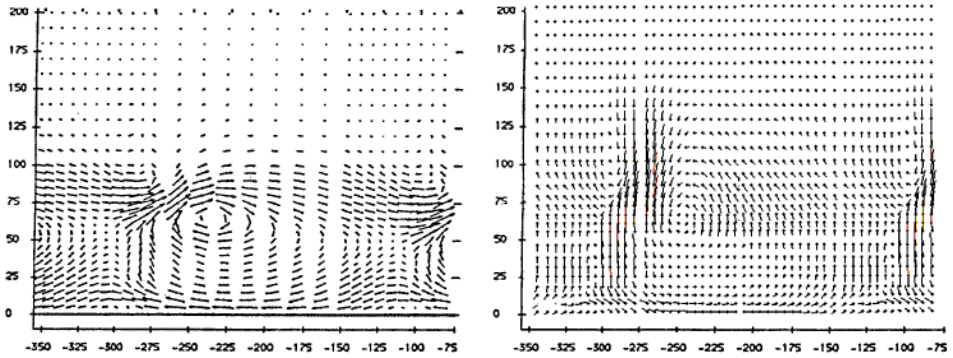

Fig. 2. DLSTC - comparison of experimental (left) and computed (right) secondary flow velocities at slot 10.

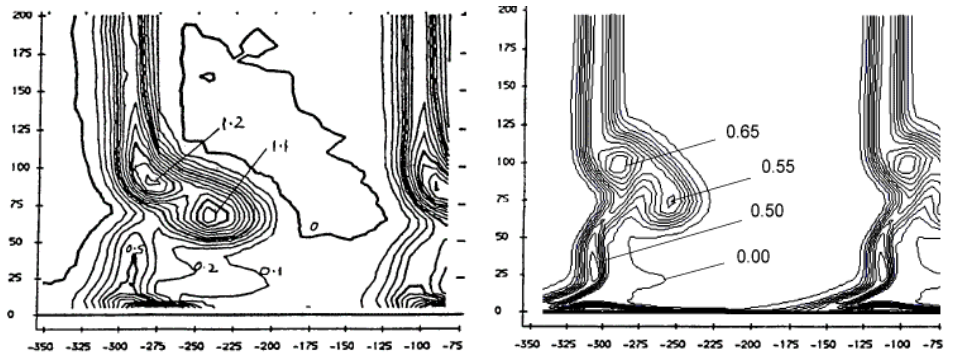

Fig. 3. DLSTC - comparison of experimental (left) and computed (right) contours of total pressure coefficient at slot 10.

wise distributions of kinetic energy losses and yaw angle at slot 10 presented in Fig. 4, where the computed values of peak loss and peak underturning from the two turbulence closures are similar and remain below those of the experimental data. It seems that for low-load axial turbine cascades at design conditions both turbulence models give equal qualitative predictions of flow patterns (like the total pressure double peak for the Durham cascade), and very similar quantitative estimates of flow characteristics, see Lampart et al [9].

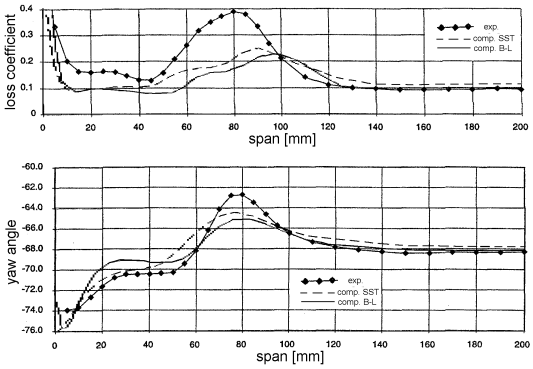

Fig. 4. DLSTC – comparison of experimental and computed - with Baldwin-Lomax (B-L) and Menter (SST) turbulence models – span-wise distribution of kinetic energy losses and yaw angle at slot 10.

4. NASA ROTOR37

Rotor37 is a transonic compressor with a design total pressure ratio about 2.1, low stability margin - 8% from the choking mass flow rate, and high rotational speed 17188.7 rpm. The data for this compressor are given by Reid & Moore [10]. Fig. 5 displays Mach number contours at the mid-span section for the choke flow and 98% of the choking mass flow rate. For the choke flow, the flow pattern consists of two shocks - a bow shock with some reflection and a closure shock. This pattern is observed to change unfavourably with the decreasing flow rate to obtain a single strong bow shock with a large after-shock separation for 98% of the choking mass flow rate. This may explain why the compressor has the maximum efficiency near the choke flow conditions, see also Denton [11]. The computed pressure-ratio-and-efficiency-versus-mass-flow-rate characteristics show a good agreement with the experimental data, see Fig. 6.

The illustrated computations were made here with the help of the Menter SST turbulence model on a grid of 200 000 nodes. The computations of Rotor37 with the help of the algebraic closure of Baldwin-Lomax are also possible, especially near design and choke flow conditions, however at near stall conditions may lead to severe convergence problems. This is expected to be mainly due to the inability of algebraic closures to handle strong adverse pressure gradient flows and separations, that is the flow features where the alternatively used SST turbulence model is believed to give improved predictions over standard two-equation models (k-ε and k-ω).

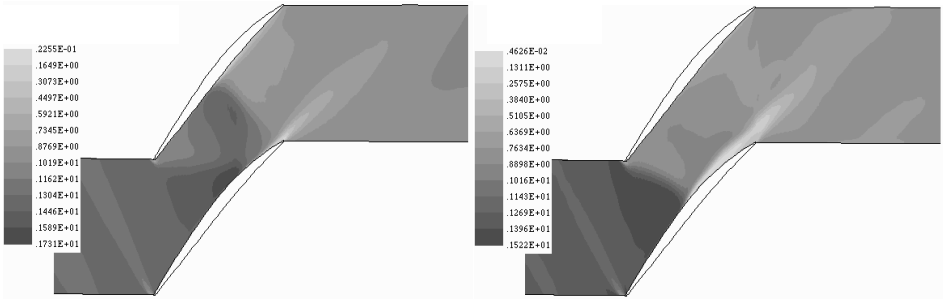

Fig. 5. Rotor37 – computed Mach number contours at mid-span for choke flow (left) and 98% of choking mass flow rate (right)

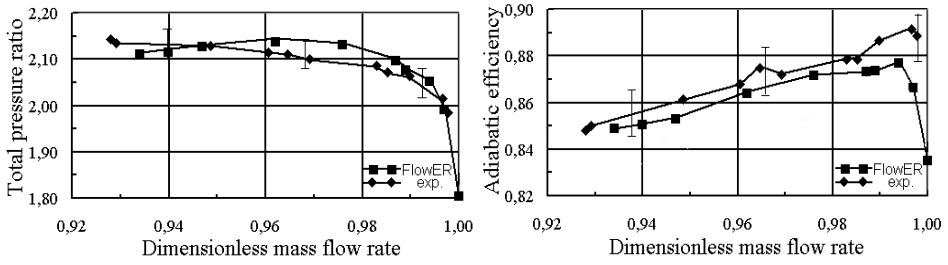

Fig. 6. Rotor37 - total pressure ratio and adiabatic efficiency versus dimensionless mass flow rate

5. NASA LOW SPEED CENTRIFUGAL COMPRESSOR

The tested centrifugal compressor is an impeller with backswept blades and vaneless diffuser, having a design mass flow rate of 30 kg/s, rotational speed 1860 rpm, measured pressure ratio 1.142 and efficiency of 92.2%. The experimental data for this compressor are given by Hathaway et al. [12], see also Kang & Hirsch [13].

Secondary flow physics in centrifugal compressors is very complex. Besides passage vortices typical for axial machines and tip leakage vortex, we can also observe Coriolis vortices due to Coriolis forces acting on hub/shroud boundary layer fluid, and blade surface vortices due to high blade meridional curvature. It is interesting to see how standard turbulence models can handle flow driven by centrifugal and Coriolis forces.

Fig. 7 shows the comparison of experimental and computed distribution of the shroud static pressure. The reference pressure is here 1 bar. The static pressure rise along the shroud is predicted well compared to the experimental data. So is the computed total pressure rise p_{1T}/p_{0T} through the compressor – 1.142 (experimental value is also 1.142), and the computed total temperature rise T_{1T}/T_{0T} – 1.044, compared to the experimental value of 1.042. The hub-to-shroud distribution of kinetic energy losses computed 20% of the shroud arc length downstream of the impeller exit is presented in Fig. 8. The computed mass averaged value is 8.6%, which gives the impeller efficiency of 91.4% - slightly underestimated compared to the experimental value of 92.2%.

Fig. 9 shows the comparison of experimental and computed velocity vectors at the pressure and suction surface of the blades. Both the experimental and computational vectors tend to turn from hub to shroud in the region where the flow turns from axial to radial. In the radial part, downstream of section 135, however, the experimental results at the pressure surface of the blade exhibit traces of flow separation from the shroud and a downstream reattachement, which is not featured in the computations.

The comparison of experimental and computed velocity isolines in three sections of the impeller is presented in Fig. 10. The velocity here is rendered non-dimensional with respect to the shroud exit velocity. At section 85, 15% of the meridional arc length downstream of the inlet, there is a tip leakage vortex in the shroud/suction surface corner – possibly too small to be seen in the experiment. Subsequent experimental pictures (section 135 - 60% and 165 – 95% of

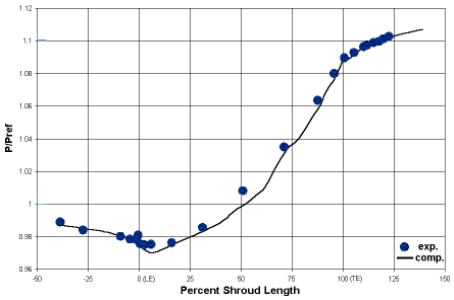

Fig. 7. LSCC - comparison of experimental and computed shroud static pressure distribution

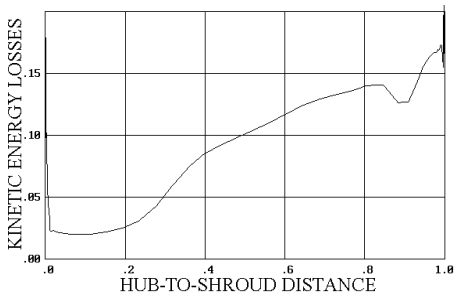

Fig. 8. LSCC – hub-to-shroud distribution of kinetic energy losses

the shroud arc length downstream of the inlet) exhibit the movement of the tip vortex towards the pressure surface, and then most likely (see Kang & Hirsch [13]) its migration towards mid-span under the condition of growing passage/Coriolis vortex at the shroud and growing pressure surface vortex. Basically, this process can also be observed from the respective computed pictures, but the extension of the computed vortex structure seems to be largely overpredicted. Also at the all presented sections (and more clearly at the pictures of secondary flow vectors, not shown here for the lack of space), experimental and computed isolines show traces of development of the pressure and suction blade vortices – overpredicted in the computations at upstream sections.

The present computations of the centrifugal impeller were made with the help of the Menter SST turbulence model on a grid of 450 000 nodes. The computed predictions of pressure and temperature rise, as well as the flow efficiency compare relatively well with the experimental data. Qualitatively, a majority, but not all, flow features observed experimentally can be obtained numerically. Further study on modelling turbulence in centrifugal and Coriolis force driven flows is needed to find quantitative agreement between experimental and computed data.

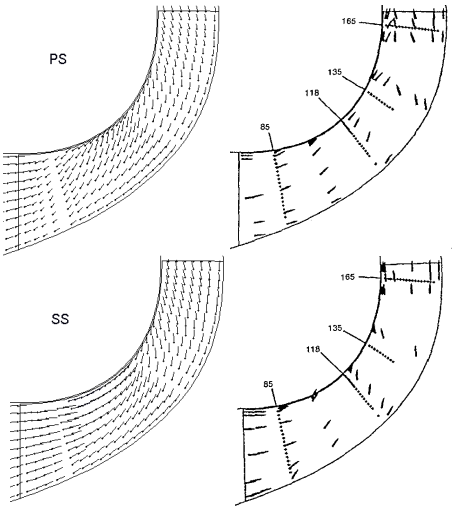

Fig. 9. LSCC - comparison of computed (left) and experimental (right) velocity vectors at blade pressure (top) and suction (bottom) surface

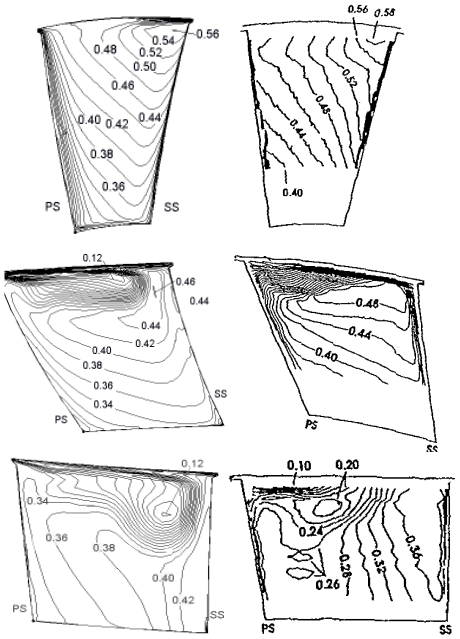

Fig. 10. LSCC - comparison of computed (left) and experimental (right) velocity isolines in sections 85 (top), 135 (centre), 165 (bottom) as denoted in Fig. 9.

6. CONCLUSIONS

The 3D RANS solver FlowER with two turbulence models – algebraic model of Baldwin-Lomax and two-equation shear stress transport model of Menter – is validated on three typical turbomachinery test cases: a Durham low speed turbine cascade, transonic NASA compressor Rotor37, and NASA low speed centrifugal compressor.

For the Durham cascade, the solver predicts well blade pressure distributions.

The total pressure double peak can be predicted using the Baldwin-Lomax model. However, values of peak losses and underturning remain underestimated. The Menter SST model does not yield a much better prediction of flow patterns in this turbine cascade.

Shock wave patterns, pressure ratio and efficiency versus mass flow rate characteristics for the NASA Rotor37 are predicted well using the solver with the Menter SST model. The computations of Rotor37 with the Baldwin-Lomax model are also possible, however at near stall conditions may lead to severe convergence problems.

The computed pressure and temperature rise, as well as the flow efficiency of the NASA low speed centrifugal compressor, compare reasonably well with the experimental data. Numerical calculations using eddy-viscosity models can predict most of the experimentally observed flow patterns, but only qualitatively, not quantitatively. Further study on modelling turbulence in centrifugal and Coriolis force driven flows is needed to find quantitative agreement between the experimental and computed data.

REFERENCES

[1] Proc. ERCOFTAC Seminar and Workshop on Turbomachinery Flow Prediction I-VIII, 1993-2002.
[2] QNET-CFD Network Newsletter, Vol.1, No. 1-3, 2001-2002.
[3] Yershov S., Rusanov A., 1996, The application package FlowER for the calculation of 3D viscous flows through multi-stage turbomachinery, Certificate of state registration of copyright, Ukrainian state agency of copyright and related rights, February 19, 1996.
[4] Baldwin B.S., Lomax H., 1978, Thin layer approximation and algebraic model for separated turbulent flows, AIAA Paper, No 78-257.
[5] Menter F.R., 1994, Two-equation eddy-viscosity turbulence models for engineering applications, AIAA J., Vol. 32, No. 8, pp. 1598-1605.
[6] Yershov S.V., 1994, The quasi-monotonous ENO scheme of increased accuracy for integrating Euler and Navier-Stokes equations, Math. Modelling, Vol. 6, No. 11, pp. 58-64 (in Russian).
[7] Yershov S.V., Rusanov A.V., Gardzilewicz A., Lampart P., Świrydczuk J., 1998, Numerical simulation of viscous compressible flows in axial turbomachinery, TASK Q., Vol. 2, No. 2, pp. 319-347.
[8] Gregory-Smith D., 1993-2002, Proc. ERCOFTAC Seminar and Workshops on Turbomachinery Flow Prediction I-VIII.
[9] Lampart P., Swirydczuk J., Gardzilewicz A., 2001, On the prediction of flow patterns and losses in HP axial turbine stages using 3D RANS solver and two turbulence models, TASK Quarterly, Vol. 5, No. 2, pp. 191-206.
[10] Reid L., Moore R.D., 1978, Design and overall performance of four highly-loaded high-speed inlet stages for an advanced high-pressure ratio core compressor, NASA TP 1337.
[11] Denton J.D., 1996, Lessons from Rotor 37, Proc. 3rd Int. Symp. Aerothermodynamics of Internal Flows, Sept. 1996, Beijing, China, pp. 3–14.
[12] Hathaway M.D., Chriss R. M., Wood J.R., Strazisar A.J., 1993, Experimental and computational investigation of NASA low-speed centrifugal compressor flow field, Trans. ASME J. Turbomachinery, Vol. 115, pp. 527-535.
[13] Kang S., Hirsch C., 1999, Numerical investigation of the three-dimensional flow in NASA low-speed centrifugal compressor impeller, Proc. 4th ISAIF, Dresden, Germany, August 31-September 2, Vol. I, pp. 274-284.